Chapter 12

Sol-Gel Glass Coating Synthesis for Different Applications: Active Gradient-Index Materials, Microlens Arrays and Biocompatible Channels

Ana Isabel Gómez Varela, María Aymerich,
Daniel Nieto García, Yolanda Castro Martín,
Pieter A.A. de Beule, Ezequiel Álvarez,
Carmen Bao-Varela and María Teresa Flores-Arias

Additional information is available at the end of the chapter

http://dx.doi.org/10.5772/67830

Abstract

The intent of this chapter is to review the use of sol-gel processing of silica and silica-titania optical coatings in recent research by the authors in three different areas: the synthesis of active gradient-index (GRIN) materials by multilayer deposition of erbium- and ytterbium-doped silica-titania films, the improvement of the optical and morphological qualities of microlens arrays fabricated by laser ablation and the functionalization of polydimethylsiloxane (PDMS) channel preclinical devices. Through the use of sol-gel, layers with specific properties can be produced. In this regard, undoped and erbium- and ytterbium-doped SiO_2-TiO_2 films have been produced and characterized using atomic force microscopy (surface topography evaluation) and spectral ellipsometry (determination of optical constants, thickness and porosity of the films). In a second application, a silica sol has been synthesized to coat microlens arrays fabricated by laser ablation. The deposited layer reduces the surface roughness of the microlens array, which yields the improvement of the contrast and the homogeneity of the foci. Finally, PDMS channels fabricated with laser technologies and soft-lithography methods are coated with a sol-gel-derived silica film to avoid the degradation of the material with organic solvents, and their biocompatibility is studied.

Keywords: sol-gel, dip coating, gradient-index media, rare-earth doping, laser writing technique, laser microfabrication, microlens arrays, PDMS devices, cell adhesion

1. Introduction

This chapter reviews the exploration of sol-gel chemical route for different applications. In particular, the synthesis of active gradient-index (GRIN) optical materials and the improvement of the optical qualities of microlens arrays as well as a better functionalization of the polydimethylsiloxane (PDMS) channel preclinical devices are presented. Sol-gel chemistry offers some unique opportunities for the synthesis of optical materials over existing production methods [1–4]. The process allows excellent control of its purity and composition since it starts with pure materials. In addition, one important advantage of the sol-gel process related to the synthesis of these types of materials is that coatings with high optical quality using low sintering temperature can be obtained. The decrease of the sintering temperature is crucial with a view to possible future industrial application.

GRIN materials are characterized by a refractive index distribution that varies spatially in a controlled manner [5]. They are typically manufactured by ion-exchange process [6, 7], although their fabrication has also been accomplished by neutron irradiation [8], chemical vapour deposition (CVD) [9] and sol-gel techniques [10, 11]. Sol-gel allows the incorporation of dopants such as rare-earth elements in an easy way. The ability to induce specific optical properties in a material by simply selecting a deliberate dopant is one of the most important advantages of sol process when it comes to the fabrication of active optical media [12–14]. In this regard, different erbium- and ytterbium-doped films based on SiO_2-TiO_2 systems have been prepared. The fabrication and characterization of monolayers with controlled properties is the first step towards the preparation of active GRIN materials. It is performed by growing successive layers until a multilayer stack described by a complex parabolic-like refractive index profile distribution is obtained [15]. These types of materials are very interesting for laser beam shaping purposes [16].

Sol-gel layers can also be used to optimize the optical and morphological properties of microlens arrays, which can be found in many modern optical devices. There are several important applications of microlens arrays, encompassing fibre couplers in optical communications systems, viewing optics, laser beam shaping elements, charge-coupled device cameras and so on. Microlenses can be fabricated by several methods, such as thermal reflow forming, stereolithography technique, mould insert, pressure difference or decompression method and hot embossing [17–20]. The majority of these methods are appropriated to produce microlenses on photoresist. Nevertheless, in recent years, the fabrication of glass-based microlenses is attracting special attention since it is widely used in photonic systems [21, 22]. Microlenses on glass can be obtained using the laser direct-writing technique, which presents some significant advantages over conventional methods: flexibility in terms of surface shapes, diameter and focal length; the very small dead space between lens lets of any desired shape and profile; and the simplicity of the fabrication setup [23, 24]. But the laser direct-writing technique is in general not able to produce microlenses with comparable imaging and stray light properties to other conventional methods. Hence, in this chapter, a silica sol-gel layer is deposited onto the micro-optical device to reduce the damage created on the glass during the laser ablation process and to enhance the optical properties of the microlens by increasing the quality of the interstices among the microlens of the array. The addition of the sol-gel thin film yields to microlens arrays with comparable imaging and stray light properties to other techniques, preserving at the same time the

http://dx.doi.org/10.5772/67830

main advantages of the laser direct-writing technique, including flexibility in terms of design, fast prototyping, low cost, non-contaminant, repeatability, etc.

Furthermore, sol-gel thin film processing can be used to enhance the lifetime of PDMS preclinical devices. PDMS is a polymer widely used for the fabrication and prototyping of fluidic chips. It can be employed for mimicking blood vessels and may be employed in biomedical primarily assays due to: (i) its transparency, which facilitates the observation of contents in channels by direct visual inspection or through a microscope; (ii) its biocompatibility; (iii) it can be coated, which allows the fabrication of PDMS multilayer devices and the integration of micro valves; (iv) its deformability; and (v) its cost-effectiveness [25]. Nonetheless, it also presents one important disadvantage as material degradation is caused when using organic solvents for cleaning, which makes the device non-reusable. This can be overcome by simply coating the PDMS chip with one or more sol-gel layers. This procedure provides the structure with the chemical robustness of the glass and preserves the biocompatibility and transparency properties without significantly altering the geometry of the PDMS device [26, 27]. In this chapter, the fabrication of PDMS devices coated with different sol-gel compositions to overcome the deterioration problem is presented. Additionally, the biocompatibility of each device is determined by evaluating cell adhesion effectiveness of human umbilical vein endothelial cells (HUVECs) cultured onto the coated channels [28].

The remainder of this chapter is organized as follows: in Section 2, the sol-gel synthesis and film deposition method are introduced. Section 3 presents the experimental procedure and methods for the fabrication of sol-gel-derived active GRIN media, microlens arrays by laser ablation and the subsequent functionalization of the micro-optical devices via sol-gel, as well as for the enhancement of the lifetime of PDMS preclinical devices. Characterization techniques and results are also described in this section. Finally, Section 4 draws the main research findings.

2. Sol-gel synthesis and film deposition

2.1. Sol-gel preparation

SiO_2-TiO_2 and SiO_2 thin films were prepared via sol-gel route for different applications. The sol compositions and their corresponding molar ratio concentration are listed in **Table 1**.

SiO_2-TiO_2 thin layers have been produced using methyltriethoxysilane (MTES, $CH_3Si(OCH_2CH_3)_3$, 98%, ABCR GmbH & Co., Karlsruhe, Germany) and titanium isopropoxide (TISP, $Ti[OCH(CH_3)_2]_4$, 97%, ABCR GmbH & Co., Karlsruhe, Germany) as precursors of silica and

Sol	Molar ratio	H_2O/alkoxides	Alkoxides/A_cH	C (g_{oxides}/L)
MTES:TISP	70/30	1.5	1	100
MTES:TISP	80/20	1.5	1	100
MTES:TEOS	60/40	1.75	4	180

Table 1. Composition, molar ratios and concentration of SiO_2-TiO_2 and SiO_2 sols described in this chapter.

titania, respectively (MTES/TISP sol). Both SiO_2 and TiO_2 are widely used in optics and photonics applications mainly due to the wide spectral region of transparency from the visible to the infrared, thermal stability and chemical durability. The MTES/TISP sol preparation is accomplished as follows: in the first stage, MTES is pre-hydrolysed using ethanol as solvent. HCl (0.1N) was then added with stirring for 1 h at room temperature. On the other hand, titanium isopropoxide is complexed by mixing with ethanol and glacial acetic acid. This solution is maintained under agitation process for 1 h. Then, the resulting solution is mixed to the MTES sol and distilled water is added, drop by drop, to complete the hydrolysis process.

On the other hand, hybrid SiO_2 sol was made from MTES and tetraethoxysilane (TEOS, $Si(OCH_2CH_3)_4$, 99%, ABCR GmbH & Co., Karlsruhe, Germany) in the molar rate 60/40 (MTES/TEOS sol). In this case, a two-step sol is prepared at ambient atmosphere by mixing TEOS and MTES with absolute ethanol followed by addition of acidulated water (0.1 M AcH) drop by drop. Next, distilled water is incorporated to the sol, which is then refluxed in a water bath at 40°C for 2 h under continuous magnetic stirring.

2.2. Dip-coating technique

Sol-gel is one of the simplest and most commonly used routes to obtain thin films with a huge variety of inorganic, hybrid and nanocomposite materials. It allows a high degree of control of the critical parameters and enables a flexibility that cannot be obtained using other conventional techniques given that it permits to coat a wide variety of substrates and complex geometries, including substrates with holes or intricate shapes. Several wet thin film coating methods exist, including dip-coating, spin-coating, spray-coating and flow-coating techniques, among others. The stages of dip coating [29] are schematically represented in **Figure 1**. Basically, the process, which is performed under well-controlled temperature and

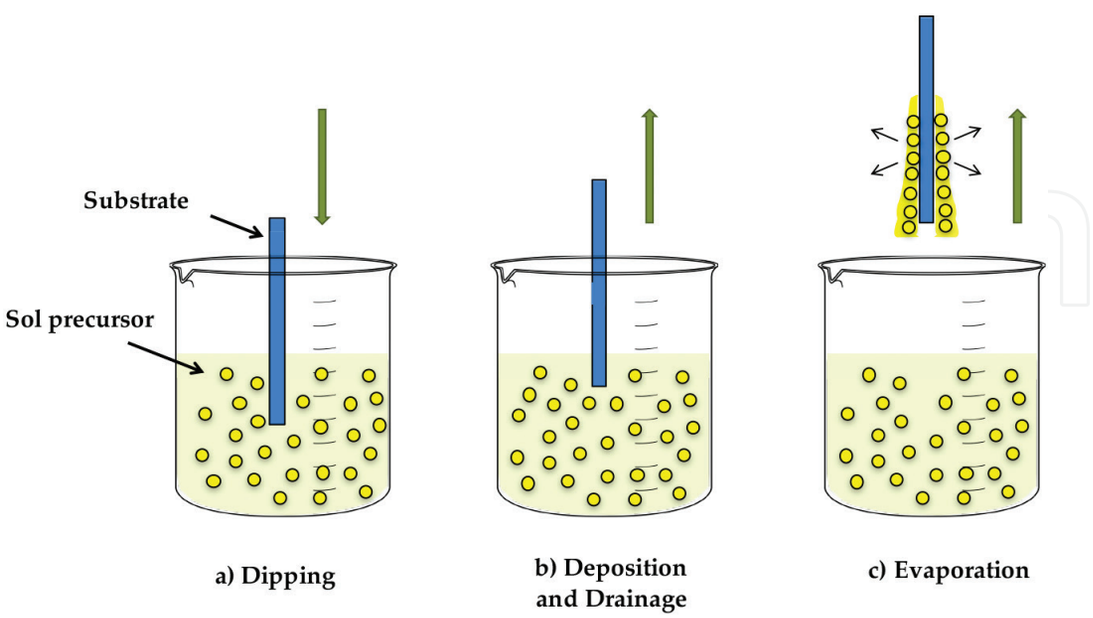

Figure 1. Sequential stages of the dip-coating technique for thin film deposition: (a) the substrate is dipped and immersed in the sol precursor, (b) the substrate is withdrawn at constant speed rate, and (c) solvent evaporation yields to the gelation of the layer.

http://dx.doi.org/10.5772/67830

atmospheric conditions, starts by immersing the substrate to be coated in the initial solution, being subsequently withdrawn at a constant withdrawal speed. Precisely, the control on the withdrawal speed and on the evaporation conditions makes possible a fine-tuning of the film characteristics, including thickness, optical constants and inner structure. The combined effects of viscous drag and capillarity action yield to the solution homogeneously spreading out along the surface of the substrate. In the final stage of the process, evaporation occurs and brings gelation of the film. Usually, a post-heat treatment is applied to the coated substrates, which also influences the characteristics of the films.

3. Sol-gel glass coating synthesis and characterization for different applications

3.1. Active gradient-index optical materials

Active gradient-index optical materials can be used as beam shaping transforming devices with gain or loss. In particular, an active GRIN material, characterized by a parabolic and complex refractive index profile, can turn an input laser beam described by a Gaussian irradiance profile into a beam with a uniform irradiance distribution [16]. **Figure 2** shows the basis of the beam shaping operation by an active GRIN medium. The input Gaussian beam impinges in the active medium and travels through the material up to the beam shaping distance. At this beam shaping distance, which corresponds to the output face of the GRIN medium, the original beam is turned into a nearly uniform beam. If the material has gain, an amplified uniform beam is obtained (a); on the contrary, if the material has loss, the beam suffers from attenuation after propagating in the medium (b).

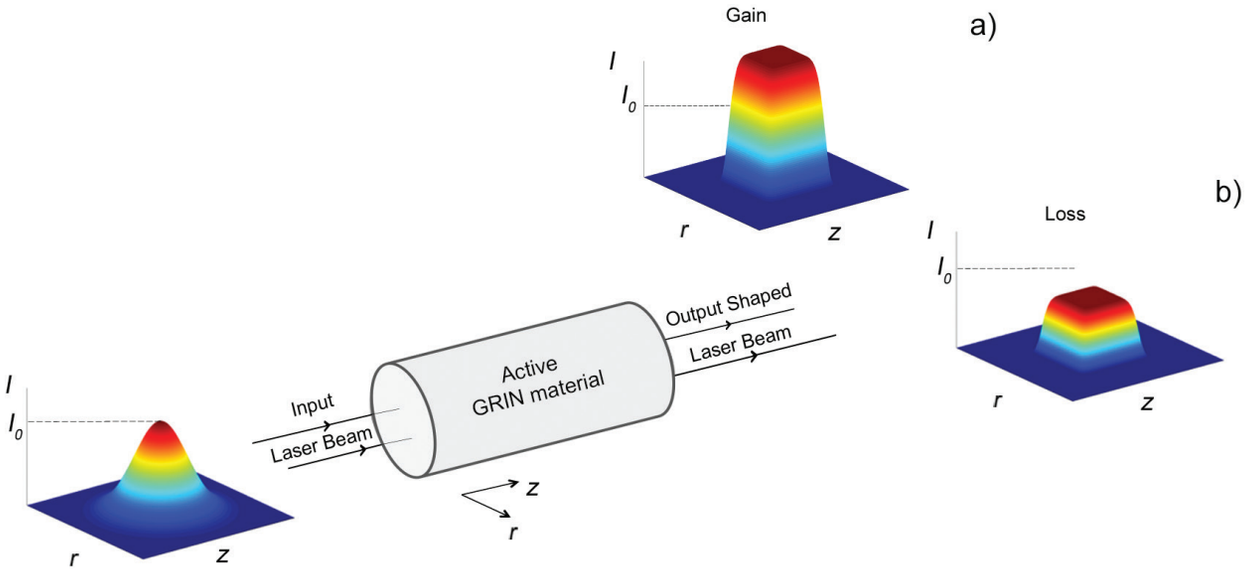

Figure 2. Schematic representation of Gaussian-to-uniform beam shaping operation by an active GRIN material with (a) gain and (b) loss. I_0 is the on-axis irradiance value of the Gaussian beam.

3.1.1. Materials and methods

A series of undoped and Er^{3+}- and Yb^{3+}-doped $70SiO_2$-$30TiO_2$ films with good optical (homogeneous) and mechanical (crack-free) properties were prepared using MTES and TISP (precursors of silica and titania, respectively) in acid conditions. The synthesis was performed in two steps following the indications provided in Section 2.1. In both erbium- and ytterbium-doped sols synthesis, the rare-earth (RE) precursor is added to the mixture after the distilled water and then maintained under vigorous stirring for 1 h. The atomic percentage of erbium nitrate pentahydrate ($Er(NO_3)_3 \cdot 5H_2O$, 99.9%, ABCR GmbH & Co., Karlsruhe, Germany) and ytterbium nitrate pentahydrate ($Yb(NO_3)_3 \cdot 5H_2O$, 99.9%, ABCR) precursors was varied between 0.3 and 2.0 at.% and 0.3 and 1.0 at.%, respectively. Previously to film deposition, commercial glass slides were washed in distilled water, dried and finally washed in ethanol. Films were deposited by dip-coating technique using a withdrawal rate of 10, 20, 30, 40 and 50 cm/min. To obtain the final samples, the sol-gel-derived films were heat treated at 450°C for 30 min using a ramp rate of 10°C/min in air atmosphere.

Selected samples were analysed by using a spectral ellipsometry (SE), an indirect method for thin film characterization, where the change of polarization of an incident light upon reflection with the material is measured. In this work, ellipsometry measurements were performed using a spectral ellipsometer (M-2000UTM, J.A. Co., Woollam) to characterize the films deposited onto glass slides. The spectra were taken in the wavelength range of 400 and 1000 nm at incident angles of 65, 70 and 75 degrees. A Cauchy model was used to fit the data obtained with WVASE32 software. On the other hand, the topographical features of the erbium-doped samples under atomic force microscopy (AFM) for a scan area of 5 μm are shown in **Figure 7**. The instrument used was a Bruker Dimension Icon® atomic force microscope operated under intermittent contact mode in air at a line scan rate of 1–2 Hz. The cantilever tip had a height of 10–15 μm and a radius of 10 nm. Typical cantilever resonance frequency varied between 350 and 367 kHz at force constants between 20 and 80 Nm^{-1}. Tapping mode images were analysed using the Gwyddion software (gwyddion.net).

3.1.2. Results

SE investigation of the films was performed in order to determine the optical constants (refractive index and extinction coefficient) and thickness of the films. As can be seen in **Figure 3**, the film thickness increases when increasing the withdrawal rate for both erbium- and ytterbium-doped samples, as well as for undoped samples. It is also interesting to note that film thickness significantly increases with dopant concentration, an effect observed by Bruynooghe et al. in 1997 [30] and attributed to the increase of the viscosity of the sol with increasing erbium concentration. The spectral dependence of refractive index and extinction coefficient of erbium- and ytterbium-doped silica-titania films are displayed in **Figure 4**. Representative films were obtained using a withdrawal rate of 20 cm/min for SiO_2-TiO_2 coatings and 10 cm/min for Er and Yb-SiO_2-TiO_2 coatings. Figure shows that the refractive index diminishes with dopant concentration (**Figure 4a** and **c**). It shows that positive values of k are obtained in the wavelength range from 400 to 1000 nm. These values can be used for the fabrication of active GRIN media with loss. For the erbium-doped samples, the graphs reveal that the 2.0 at.% Er-doped

http://dx.doi.org/10.5772/67830

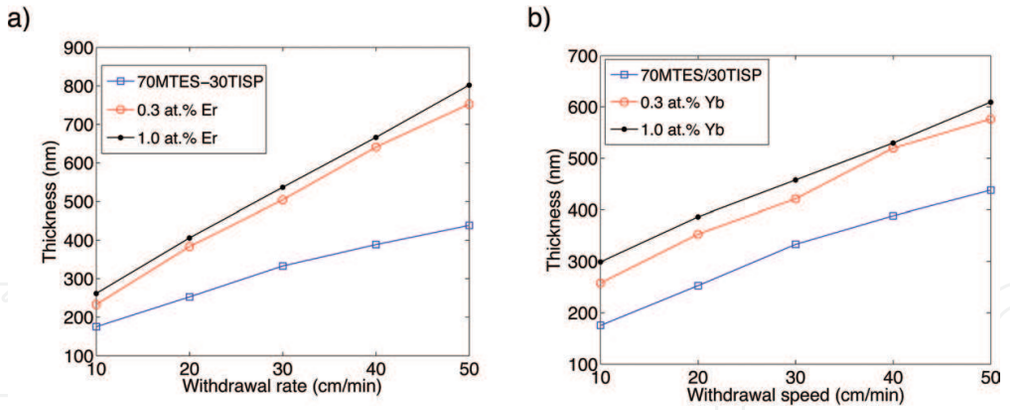

Figure 3. Thickness of the rare-earth-doped 70MTES/30TISP thin films versus withdrawal rate obtained with SE: (a) erbium-doped films and (b) ytterbium-doped films.

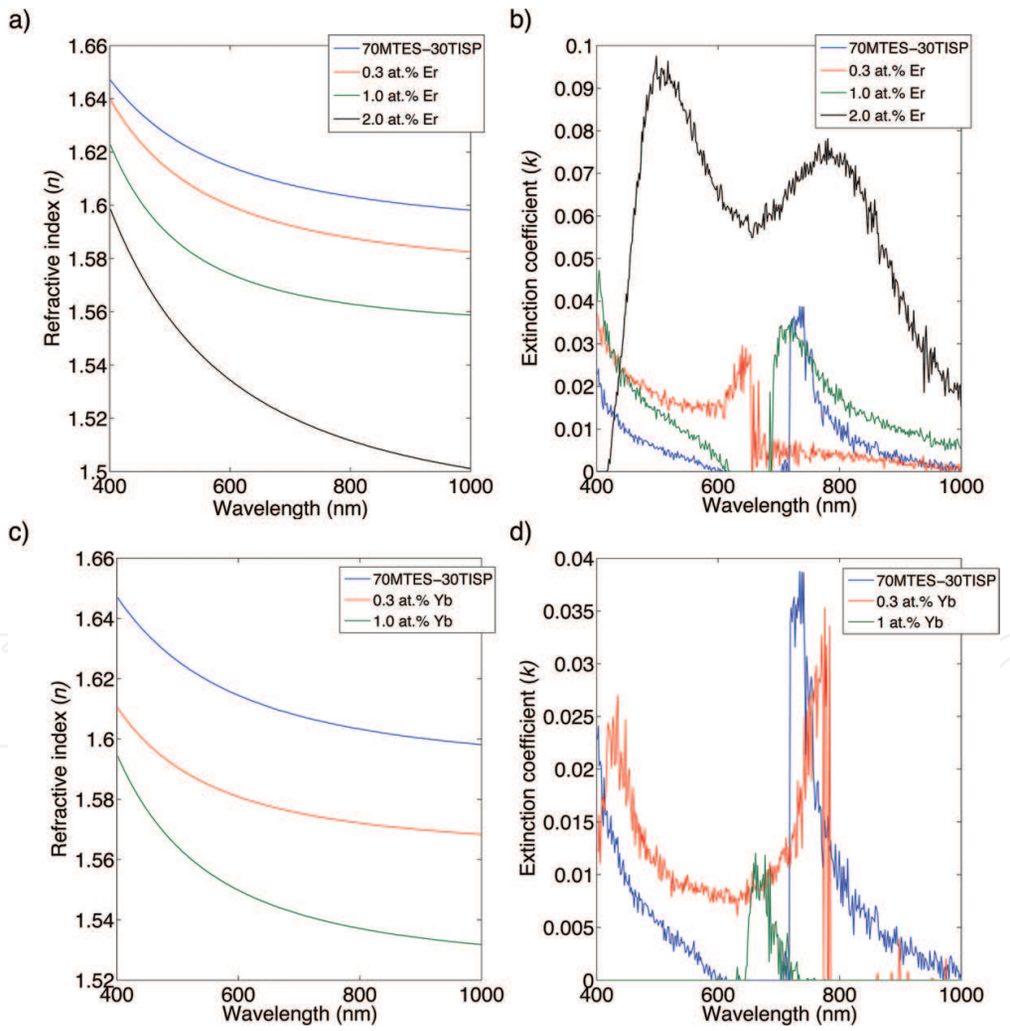

Figure 4. Optical constants of the erbium-doped (top) and ytterbium-doped (bottom) films measured by means of spectral ellipsometry compared to undoped silica-titania film: (a) and (c) refractive index and (b) and (d) extinction coefficient.

film presents the highest value of *k* along the whole spectral range, factor that probably occurs because of the dissimilitude of its surface morphology compared to the other deposited layers. With regard to ytterbium-doped samples, it can be found that for the higher doped film, *k* is close to zero along the whole measuring wavelength interval and achieves its maximum value around 650 nm. The measured values of the extinction coefficient evidence that for the SiO_2-TiO_2 film, *k* reaches its maximum value at ca. 750 nm and it is slightly shifted to the right for 1 at.% Yb-doped silica-titania film, reaching a maximum at approximately 800 nm. For both samples, the extinction coefficient shows a similar behaviour.

For both erbium- and ytterbium-doped samples, the refractive index was found to decrease appreciably when increasing dopant concentration but to remain below the undoped SiO_2-TiO_2 film (see **Figure 4**). This feature suggests that the porosity of the coatings increases with rare-earth concentration. Porosity percentage of the films can be determined using the following expression [31, 32]:

$$\Pi = 1 - \left(\frac{n_p^2 - 1}{n_p^2 + 2} \Big/ \frac{n_b^2 - 1}{n_b^2 + 2} \right) \quad (1)$$

where n_p and n_b represent the refractive index of the undoped silica-titania film (reference film) and the refractive index of the doped film, respectively. This equation assumes that the pores of the coating are filled up solely with air. Hence, the porosity values for the erbium- and ytterbium-doped films were determined from the measured refractive index with spectral ellipsometry at λ = 633 nm as function of dopant concentration and listed in **Table 2**. As expected, the results demonstrate that film porosity increases with dopant concentration. In addition, higher porosity relative values are obtained for the ytterbium-doped films when the same dopant concentration is employed.

AFM measurements of the surface of the undoped and erbium-doped silica-titania films are compared in **Figure 5**, while the corresponding numerical values for the most typical roughness parameters are gathered in **Table 3**. A visual inspection of AFM images reveals no significant changes on the surface morphology of the 0, 0.3 and 1 at.% Er-doped films. In general, topographical images display irregular-shaped and randomly grown granular surfaces. On the contrary, the sol-gel-derived film prepared with the higher erbium concentration (2 at.%), whose pore size diameter was estimated to 250 nm, presents important structural changes compared to the other films. In this case a honeycomb structured porous surface is found and the size and number of porous has increased, being this feature consistent with the SE results (see **Table 2**), where an increase of the porosity with dopant concentration was evidenced. In **Table 3**, it can be observed from arithmetic roughness (R_a) and root-mean-square roughness (R_q) values that smooth surfaces are obtained and that they increase with erbium concentration. The skewness (R_{sk}) positive values expose that the surface peaks and asperities are predominant over valleys, except for the 2 at.% Er- SiO_2-TiO_2 film where the contrary factor occurs, indicating that the surface is mainly composed of valleys. In addition, kurtosis (R_{ku}) reports the sharpness of profile peaks. The values provided are larger for the undoped SiO_2-TiO_2, implying the existence of a small number of extreme heights. On the contrary, the lower kurtosis in the other samples studied indicates moderate surface height features. A similar behaviour is expected regarding Yb-doped films.

http://dx.doi.org/10.5772/67830

Er at.%	∏ (%)	Yb at.%	∏ (%)
0.3	2.0	0.3	5
1	5.4	1	10
2	11.25	–	–

Table 2. Relative porosity values of the sol-gel-derived thin films as a function of dopant concentration.

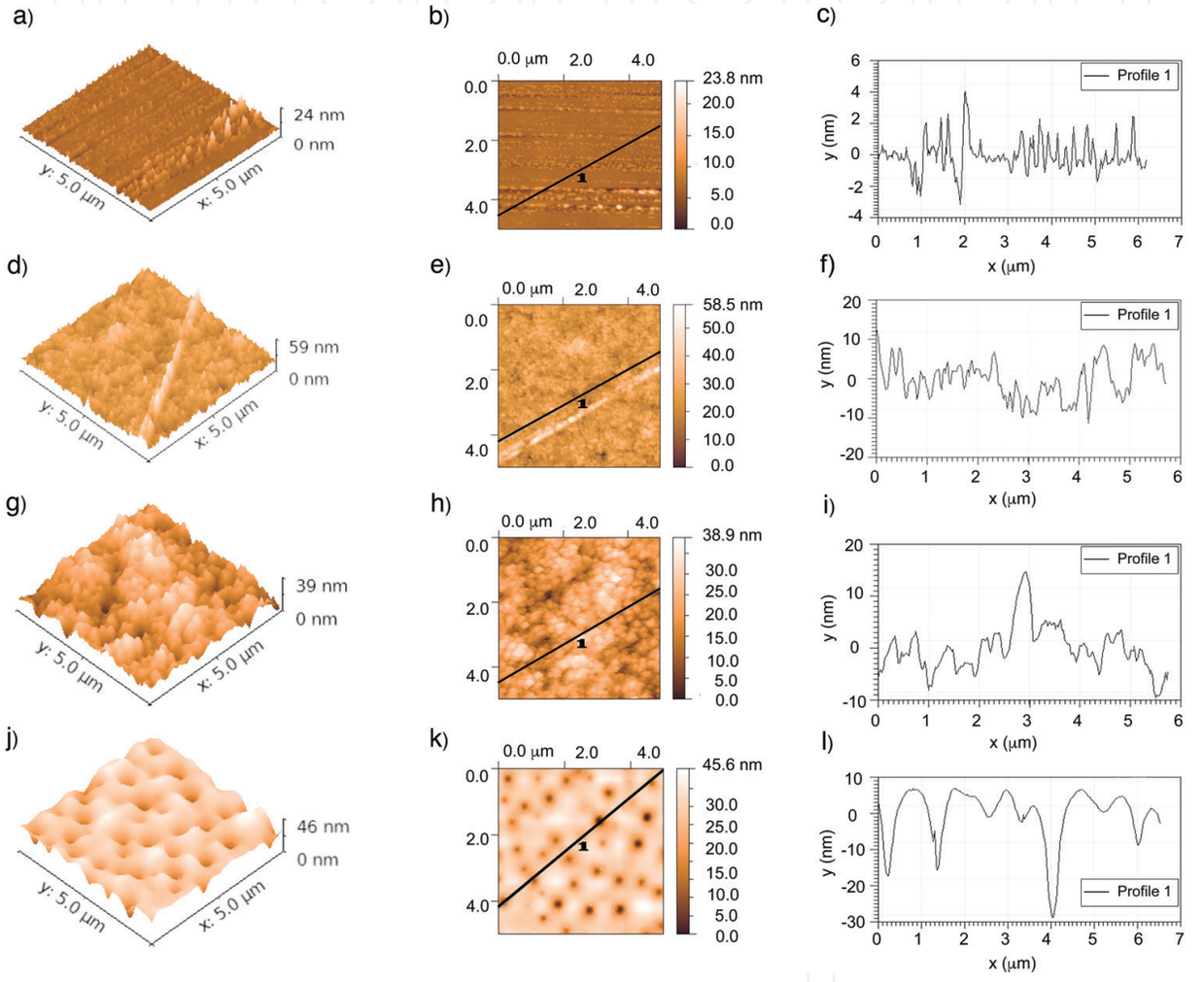

Figure 5. (a), (d), (g) and (j) 3D tapping mode in air AFM images of the thin films prepared onto a commercial glass substrate by sol-gel dip coating with (b), (e), (h) and (k) respective surface morphology and (c), (f), (i) and (l) section profiles recorded along the black line indicated. From top to bottom: 0, 0.3, 1 and 2 at.% Er- SiO_2-TiO_2 film measurements.

3.2. Improvement of the optical and morphological properties of microlens arrays fabricated by laser using a sol-gel coating

In this section, a simple, non-contaminant and repeatable method to fabricate microlens arrays is presented. The micro-optical devices are obtained via laser ablation, and the surface

Er at.%	R_a (nm)	R_q (nm)	R_{sk}	R_{ku}
0	0.82	1.28	2.410	11.70
0.3	3.88	5.25	0.818	2.96
1	4.19	5.31	0.121	0.027
2	4.10	5.74	−1.550	3.93

Table 3. AFM principal surface roughness parameters of the Er-doped SiO_2-TiO_2 films.

roughness of these devices is reduced by depositing a sol-gel-derived silica film, which covers the interstitial spaces between consecutive microlenses. This fact provokes substantial reduction of the stray light at the focal plane of the microlenses, thus increasing their optical quality.

3.2.1. Materials and methods

A commercial float soda-lime window glass is used as substrate, which was provided by a local supplier. The dimensions of the samples were 60 mm × 20 mm × 3 mm. A previous compositional analysis of the soda-lime glass reveals the existence of tin (Sn) only in one side of the samples. This fact is related to the fabrication process of the window glass. As a result, the samples present two different faces with the presence of Sn impurities only in one of them. These impurities will be crucial during the microstructuring of the glass with the nanosecond laser [33]. Nevertheless, some researchers have demonstrated the advantages of using ultrashort femtosecond pulses for microstructuring materials [34].

Experimental setup for fabricating microlens arrays is illustrated in **Figure 6**. The microlenses were obtained on glass using Ti:Sapphire Femtosecond Amplitude Systems S-pulse HP laser operating at 1030 nm wavelength and 500 fs pulse width combined with a galvanometer system (mirror positioning system designed for laser marking) for addressing the output laser beam. The laser is focused on the glass surface with a 100 mm focal length lens. This is a flat-field lens that provides a uniform irradiance distribution over a working area of 80 × 80 mm^2. The laser scan path describes circular trenches for designing each microlens. Laser parameters were a power on the order of 0.8 W, a repetition rate of 10 kHz, a wavelength of 1030 nm, a pulse width of 500 fs and a scan speed of 160 mm/s. Different microlens arrays were fabricated according to the laser setup described in **Figure 6** and varying the number of laser passes from 1 to 5. As can be seen in the figure, each cylindrical structure is obtained by the ablation of a circular trench formed by moving the laser beam, using the galvanometer mirror system, relatively to the glass sample being maintained in the same position. A time of 10 s is taken to expose an area of 2 × 2 mm^2.

Next to the laser fabrication process, MTES/TEOS sol was prepared by sol-gel process according to the synthesis route indicated in Section 2.1. Silica coatings were deposited onto the optical elements or microlens by dip-coating technique using a withdrawal rate of 10 cm/min and heat treated at 450°C for 30 min in air atmosphere.

http://dx.doi.org/10.5772/67830

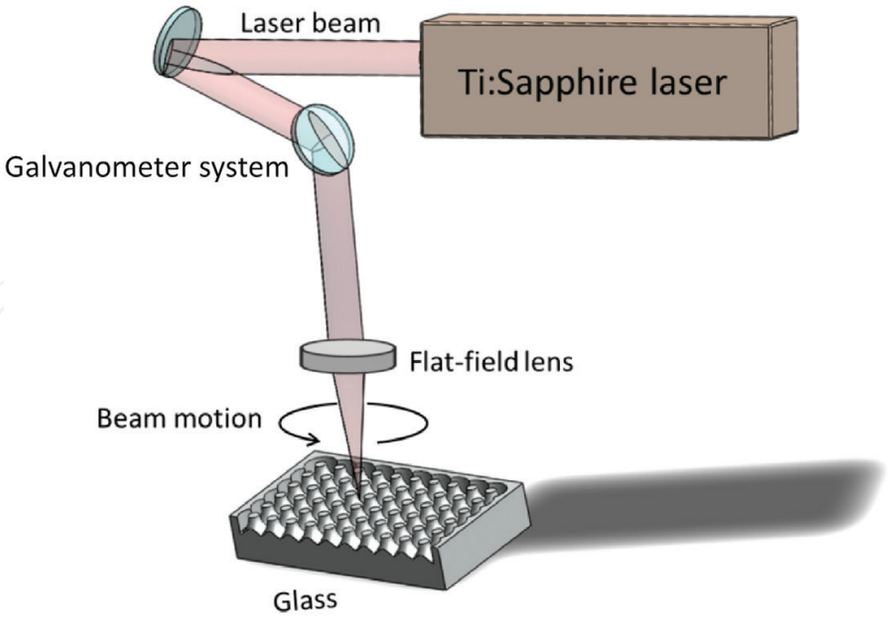

Figure 6. Experimental setup for fabricating microlens arrays.

The optical transmission of glass substrate and sol-gel coating was measured using a PerkinElmer Spectrometer (type Lambda 950 UV/Vis). The thickness and refractive index of the films were determined with the spectral ellipsometer (WVASE32, J.A. Co., Woollam M-2000UTM). Besides, the finished samples were inspected using both optical and confocal microscopes. The optical microscope Nikon MM-400 was used to visualize the sample and predetermine damage at the surface. In addition, a confocal microscope, SENSOFAR PLμ 2300, allowed us to perform topographic measurements on the surface and to obtain 3D images of the generated microlenses. The results presented were acquired using a 20XEPI microscope objective. The irradiance of the focus and the microlens spot size were determined using a beam profiler (BP-109UV).

3.2.2. Results

The topographical data acquired with the confocal microscope were used to measure the diameter, sag and roughness of microlens (see **Table 4**). **Figure 7a** shows a 3D confocal image of the microlens array fabricated by five laser passes and **Figure 7b** shows the same element after being coated with a silica sol-gel film. **Figure 7c** shows the transversal profile of one microlens and the same microlens after being coated with the sol-gel thin film. The thickness and refractive index of the SiO_2 film structure measured by SE are 1384 nm and 1.38 at 699.7 nm, respectively.

The focusing properties of the fabricated microlenses were characterized in terms of its focal length and spot size. The experimental setup for measuring the focal length of these microlenses consists of a He-Ne laser (632.8 nm), a 40X objective lens and a camera. We focused the microscope objective on the surface of the microlenses, this location was recorded, and then

	Number of laser passes		
	1	**3**	**5**
Microlenses fabricated by laser without sol-gel coating			
Diameter (μm)	38.17 ± 1.34	41.09 ± 1.46	44.08 ± 0.57
Sag (μm)	2.71 ± 0.14	10.0 ± 0.3	19.2 ± 0.4
Roughness (nm)	450 ± 13	1025 ± 34	1340 ± 25
Focal length (μm)	760 ± 10	150 ± 10	90 ± 10
Spot size (μm)	8.3 ± 0.4	5.3 ± 0.3	4.5 ± 0.2
Microlenses fabricated by laser with sol-gel coating			
Diameter (μm)	41.42 ± 1.49	41.60 ± 0.68	39.50 ± 1.48
Sag (μm)	1.39 ± 0.14	7.5 ± 0.5	17.7 ± 0.7
Roughness (nm)	23 ± 0.58	34 ± 0.26	32 ± 0.22
Focal length (μm)	820 ± 10	180 ± 10	210 ± 10
Spot size (μm)	6.2 ± 0.3	3.2 ± 0.1	2.3 ± 0.1

Table 4. Morphological and optical parameters of microlens arrays.

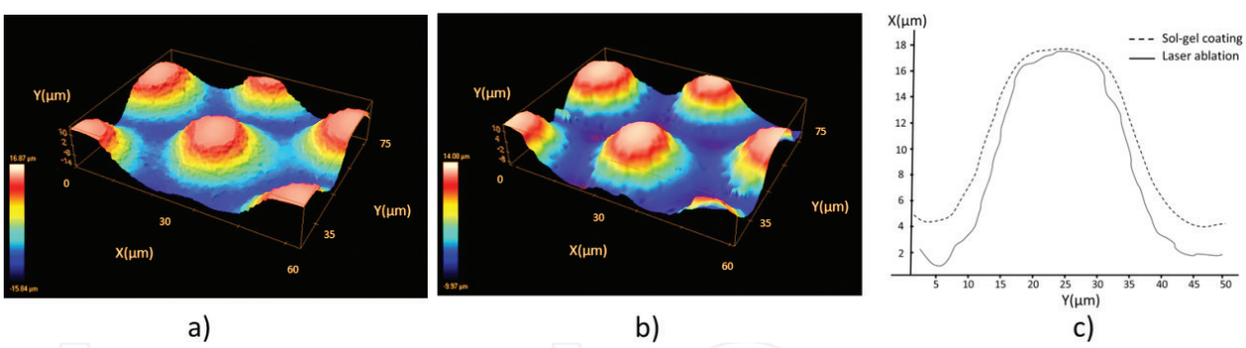

Figure 7. (a) Confocal image of one microlens array fabricated by laser ablation, (b) the same microlens with sol-gel coating and (c) profile of the microlens before (solid line) and after (dashed line) the sol-gel coating deposition.

the microscope was moved until the image of an arbitrary object is observed. The image was approximately located at the focal plane of the microlenses. The difference between these positions is a measure of the focal distance of the tested microlens arrays [35]. The data acquisition accuracy of this setup is ±5 μm. For determining the quality of focuses, the beam profiler BP109-VIS of Thorlabs was used. The focus spot size is determined by calculating the width at $1/e^2$ (see **Figure 8**).

3.3. Sol-gel coatings for PDMS device lifetime enhancement and biocompatibility

The design, fabrication and development of 3D prototypes that mimic blood vessel and lab-on-a-chip systems have aroused a huge interest in the last years due to the amount of

http://dx.doi.org/10.5772/67830

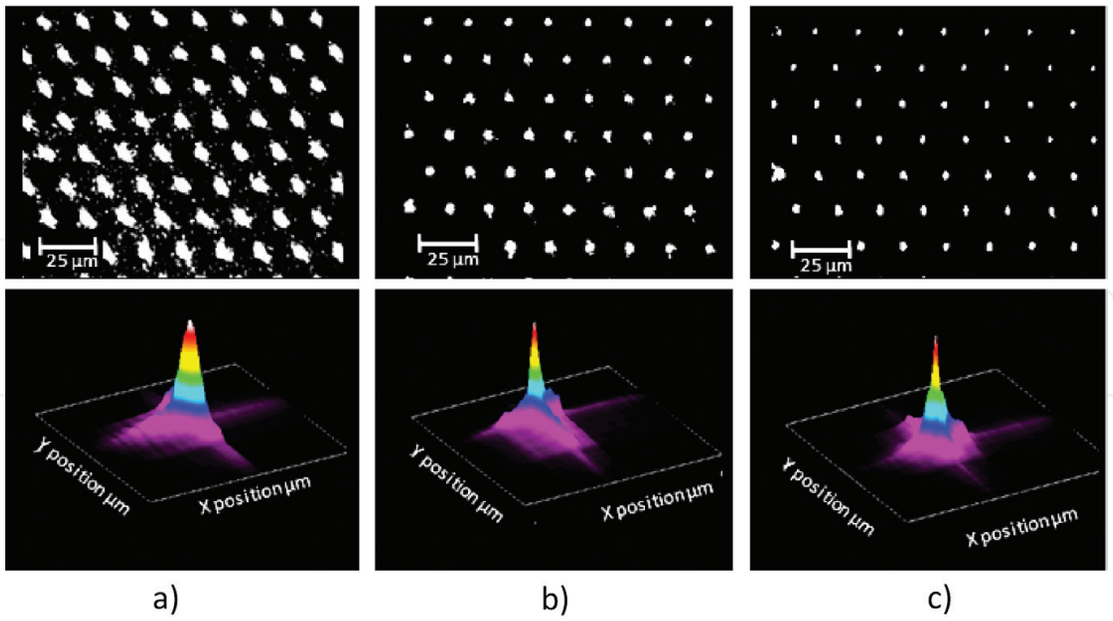

Figure 8. Focal plane image and focal irradiance distribution for the microlenses obtained at different laser passes with and without silica sol-gel coating: (a) one laser pass, (b) three laser passes and (c) five laser passes.

applications they present. By using these devices, the study of different pathologies, such as cardiovascular diseases [36] or tumour cells [37], can be performed. These experiments are carried out in controlled laboratory conditions, and the obtained results are directly linked with a better understanding of these illnesses. The structures that shape these devices can be as complex as a micron-scale laboratory or as simple as a single channel [38, 39]. Several materials have been employed for this purpose, from glass [40] to polymers [41] or silicon [42]. One of the most commonly used materials when manufacturing these devices is PDMS because of its advantages. Its permeability to gases, optical transparency, biocompatibility and replicating ability make this material very suitable for the fabrication of these preclinical chips, where cell cultures under flow conditions are performed. When using PDMS, the most common technique for the replica procedure is the soft-lithography method [25], which provides an accurate replica of the initial structure or master. For the master fabrication, techniques like lithography [43] or cutting plotter [44] have been reported, but the most promising of all is laser direct writing [45]. Its accuracy, versatility, speed and non-contact nature make it a very appropriate technique for the structuring of materials. Laser ablation can be performed in numerous materials, but glass substrates are very suitable for the master role due to its hardness and resistance [35].

As reported previously, PDMS is an optimal material for the fabrication of preclinical devices, but it presents an important disadvantage: it degrades when it is in contact with organic solvents. These solutions are very common in biomedical assays, and when PDMS is exposed to them, the device cannot be reused anymore due to the fact that it will lead to an abnormal cellular growth. Sol-gel coatings present themselves as a solution to overcome this problem by providing the structure with the robustness of the glass against these solvents but maintaining the geometry, transparency and biocompatibility of the chip [26, 27].

3.3.1. Materials and methods

Structures are commonly replicated in PDMS by using soft-lithography methods. By using this technique, a reliable replica of the initial structure or master is easily and quickly achieved. In this work, the master was fabricated over soda-lime glass using indirect laser writing technique. A Nd:YVO_4 laser (Rofin, Plymouth, MI, USA) in Q-switch mode and in the nanosecond regime was employed. This temporal regime is more implemented in industrial lasers than the femtosecond one. The laser beam has a wavelength of 1064 nm and a pulse duration of 20 ns. Laser technology allows the creation of very complex structures, but in this section, a single channel was the chosen design due to the fact that most of the microfluidic chips or preclinical devices are a combination of different channels. The laser setup was combined with a galvanometer system, conformed by mirrors that addressed the laser beam in the desired direction in order to create the structure. A 100 mm focal length flat-field lens was employed to focus the laser beam over the substrate. This lens ensures a working area of 80 × 80 mm^2. In order to obtain larger dimension channels, an indirect laser writing technique was employed. This procedure, known as laser backwriting [46], consists of focusing the laser beam on a metal target placed below the soda-lime glass substrate. The plume generated during the metal ablation process expands until it reaches the glass, and the impact of the expelled particles of the metal foil ablates the glass substrate, creating the desired structure. In this case, channels with millimetre dimensions were fabricated, so several laser passes were applied in order to obtain these structures. Laser parameters were 8 W of average power, 12 kHz of repetition rate and a scan speed of 1000 mm/s.

Due to its ablative nature, during the backwriting process, a high roughness was generated on the surface of the structure. This roughness must be reduced in order to obtain high-quality channels that allow optical microscopy inspections. For this purpose, a combined thermal technique was employed to enhance the quality of the laser-generated structures. The setup has a CO_2 laser (Easy Mark, Tinley Park, IL, USA) and a roller furnace [47]. The thermal procedure was developed as follows: the soda-lime glass master was introduced into the roller furnace and it was gradually heated. The sample was moved at 1000 mm/h and achieved a temperature of 500°C, which was below the transition temperature of the soda-lime glass but enough to avoid any cracks derived from the thermal shock that occurs when the laser beam is focused over the material surface. Once the sample was heated, the CO_2 laser beam interacted with the surface of the channel and melted the material, which was redistributed from the top of the channel to the bottom. Consequently, the roughness value of the device, as well as the depth of the channel, decreased its value. The CO_2 laser has a fundamental wavelength of 10.6 μm and a pulse duration of 10 μs, operating in the Q-switch regime. The laser beam was focused over the substrate by passing through a flat-field lens of 1 m focal length that provided a working area of 120 × 120 mm^2. Laser parameters were 12 kHz repetition rate and 90 cm/s scan speed. Channels had 2 mm width and their depths decreased from 1.215 to 1.005 mm after the thermal treatment. Once the master was fabricated by laser techniques over soda-lime glass, the channel was replicated in PDMS by following soft-lithography methods.

http://dx.doi.org/10.5772/67830

As previously mentioned, PDMS degrades when exposed to organic solvents, which are commonly employed in biomedical applications. One example is ethanol, which is frequently used for the sterilization of laboratory material. Once PDMS comes into contact with this solvent, the device becomes automatically non-reusable. If any cell culture is performed over this material, an abnormal cell growth will be observed. **Figure 9** clearly depicts this situation. In this figure, a cell culture over a PDMS channel, fabricated as it was previously described, is shown. In particular, human umbilical vein endothelial cells (HUVECs) were seeded. These cells were obtained from umbilical cords donated from the mothers after their informed consent, following the protocol approved by the Ethics Committee for Human Studies in Galicia (Spain) according to the Helsinki Declaration of 1975. In **Figure 9a**, we can appreciate the cell growth when cells were cultured over the PDMS channel for the first time. They regularly spread and form a monolayer, with the characteristic cobblestone structure of endothelial cells. **Figure 9b** presents the situation of the cell culture when the channel was reused for the third time and sterilized with ethanol between each use. The cellular behaviour is totally different from the previous one. In this case, we can appreciate how cells do not form a monolayer but instead they attach to each other, gathering in clusters and minimizing the contact surface with the degraded PDMS, leading to an abnormal cell culture and organization. Human endothelial cells were stained with green calcein acetoxy methyl (AM) (Invitrogen, Thermo Fisher Scientific, Waltham, MA, USA) for four min (incubation conditions: 37°C temperature, 95% air, 5% CO_2 atmosphere and more than 80% of humidity). Calcein is a cell-permeant dye that acts as a viability indicator by emitting in green wavelength when it is excited by fluorescence.

As previously mentioned, a possible solution to overcome this problem is the use of sol-gel. By coating the PDMS with sol-gel, we provide the channel with the robustness of the glass and the coated material does not degrade when it is exposed to organic solvents. In

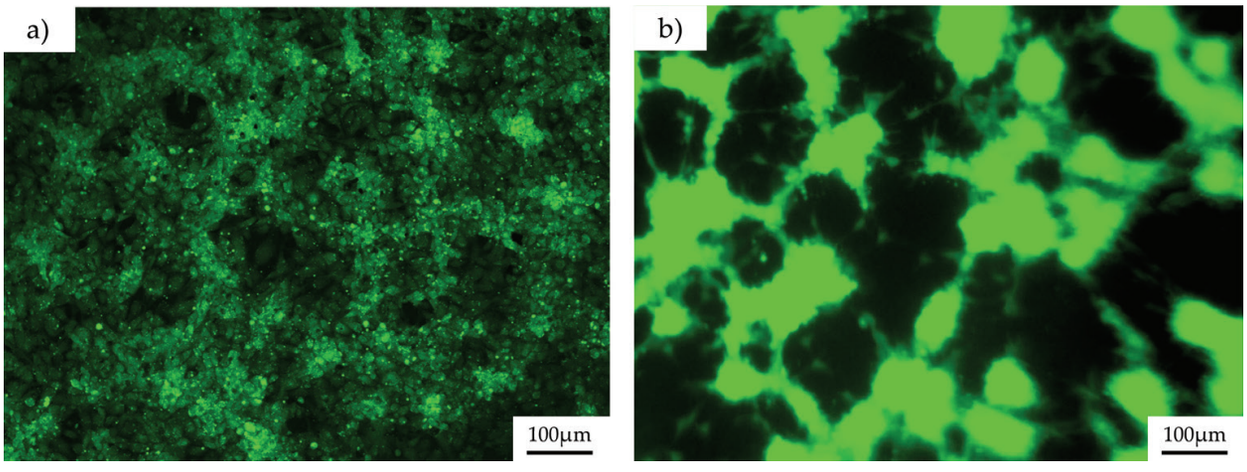

Figure 9. Fluorescence microscopy images of the human umbilical vein endothelial cells (HUVECs) seeded over PDMS channels after the (a) first and (b) third use of the device. The channel was cleaned with ethanol in between usage for sterilization purposes. HUVECs were stained with green calcein AM.

this particular case, different silica and silica-titania sol-gel coatings were applied over the PDMS structures. Hence, 60MTES/40TEOS, 70MTES/30TISP and 80MTES/20TISP compositions were employed in order to determine if they were biocompatible and if cells grew over these different coatings. The study of the differences in the cell behaviour among these compositions was also carried out. For performing the coating, the dip-coating technique was employed (see **Figure 1**). In this case, the dip-coating withdrawal speed was 6 cm/min. Before applying the post-heat treatment to the films, the substrates were allowed to dry several minutes at room temperature and then placed into a static Nanetti furnace for 2 h at a temperature of 150°C. A ramp rate of 5°C/min in air atmosphere was used to gradually heat up the sample. After the manufacturing process, it was observed that the sol-gel layer reduced the device irregularities but the original shape and dimensions of the original structure were maintained.

3.3.2. Results

Once the PDMS channels were coated with the above-mentioned compositions, HUVECs were cultured over them in order to analyse the cell behaviour over these substrates. The HUVECs were isolated and cultured following the protocol described by Rodiño-Janeiro et al. [48]. The PDMS structures were sterilized in autoclave at 120°C for 30 min and immersed in endothelial growth medium (EGM-2; Lonza Basle, Switzerland) for 30 min as pretreatment to enhance cell adhesion to the surfaces. HUVECs were dyed with calcein acetoxy methyl (AM) for determining the biocompatibility of the sol-gel compositions, since this dye only expresses in green fluorescence when cells are alive. After that, cells were washed twice in medium for removing the excess of fluorescent signal that could interfere in the image acquisition. Cells were seeded over the channels at a concentration of 10^6 cells/mL and incubated for a day. After this time, channels were washed with medium to remove non-adherent cells. The samples were observed under fluorescence microscopy and the results are shown in **Figure 10**. As calcein is a viability indicator, we can determine that all the sol-gel compositions employed are biocompatible, since cellular signal was collected by an Axio Vert A.1 Zeiss fluorescence microscope (Oberkochen, Germany). Nevertheless, there were significant differences in the growth and spreading of the HUVECs depending on the composition. The 80MTES/20TISP sol-gel coating is the most suitable environment for cells to grow and spread as we can appreciate a higher

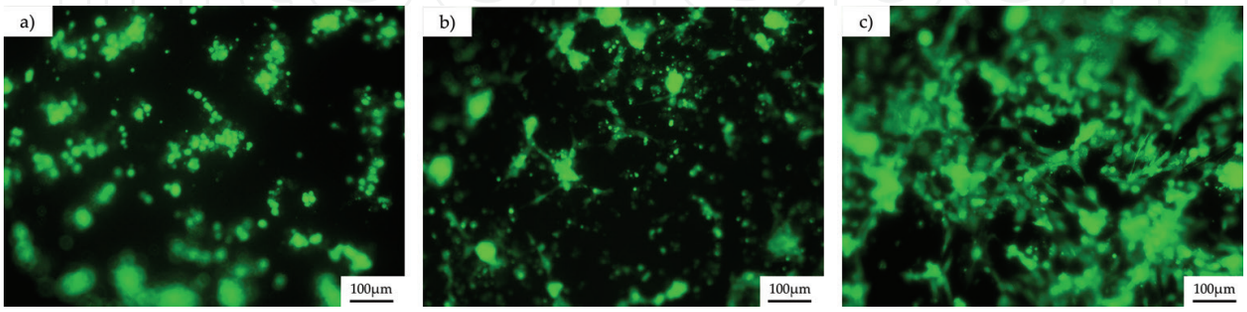

Figure 10. Fluorescence microscopy images of the human umbilical vein endothelial cells stained with calcein AM over the next sol-gel coatings: (a) 60MTES/40TEOS, (b) 70MTES/30Tisp and (c) 80MTES/20TISP after one-day culture.

http://dx.doi.org/10.5772/67830

proliferation in this case than in the others. Cell morphology was also the best; cells were spread and attempt to form a monolayer. On the other hand, the 60MTES/40TEOS composition seems to be the most hostile environment for cell growth. Cellular proliferation was low and cells presented a round shape, which suggests that the anchoring to the surface is week. The 70MTES/30TISP presents an intermediate situation where part of the HUVECs was attached to the surface. In all of the cases, we can appreciate that, even after washing, some cells remain adhered to others instead to the surface, generating an excess of fluorescent signal.

4. Conclusions

Sol-gel chemical route is suitable for the fabrication of active GRIN optical materials, for the functionalization of laser-derived micro-optical arrays as well as for the improvement of PMDS fluidic chips. Sol-gel-derived thin film multilayers may be a good approach to obtain GRIN media due to sol-gel powerfulness and versatility for tailoring the characteristics of the films. Erbium- and ytterbium-doped silica-titania films were prepared by sol-gel, finding that film thickness varied with rare-earth element concentration and increased linearly with increasing withdrawal rate of dip-coating process. The highest thickness values were achieved for larger dopant concentration. Additionally, the refractive index of the films decreased with rare-earth concentration. On account of the fact that this was only a preliminary attempt to obtain active GRIN media by sol-gel process, as to the extinction coefficient, a general trend to increase with doping concentration could be noticed, although the mechanisms of light loss in are worth original investigations. Porosity of the Er- and Yb-doped silica-titania films also increases with RE concentration. Finally, AFM images of the deposited and annealed films revealed smooth surfaces and the formation of porous granular nanostructures where valleys, mountains and island clusters became larger as dopant concentration increases.

Good-quality microlens arrays can be obtained using a combination of laser direct-writing technique and a subsequent sol-gel process. The proposed technique allows us to obtain microlens with a diameter in the range of 38–45 μm and depth in the range of 1–17 μm. The applied sol-gel silica layer reduces the surface roughness and increases the quality of the interstices between the microlenses generated by the ablation process. The obtained sol-gel-coated microlens improves the contrast and the homogeneity of the foci with respect to those uncoated. UV-Vis analysis reveals that the sol-gel layer enhances the transmission of the micro-optical element. Spectral ellipsometry measurements show that the refractive index of the deposited silica layer decreases with the increment of the wavelength, for a coated thickness of 1384 nm.

In this chapter, it has also been shown that sol-gel chemistry offers an interesting route to functionalize preclinical devices. In this regard, a technique that combines laser and soft lithography to fabricate the master and the replica of PDMS channels, respectively, was presented. Since these structures imitate blood vessel geometries, they can be used for preclinical biomedical applications. Different sol-gel coatings were deposited onto the channels in order to provide the structure with the chemical robustness of the glass and preserve the biocompatibility and transparency properties without significantly altering the geometry. Hence, HUVECs

were seeded over them to study the biocompatibility of the devices. All the coatings analysed allowed the cells to live. Additionally, the study revealed that the 80MTES/20TISP sol-gel coating was the most appropriate composition when working with HUVECs due to the stretched form of the cells and their attempt to form a monolayer, which indicates that cells were properly attached to the surface.

Acknowledgements

This work has been supported under contracts MAT2010-18519, Ministerio de Ciencia e Innovación, MAT2015-71119-R AEI/FEDER, UE, Ministerio de Economía y Competitividad, Spain, and ISCIII/PI14-01140/ FEDER, Instituto de Salud Carlos III, Spain. Ana I. Gómez-Varela acknowledges the financial support from the FPU Doctoral Fellowship (Ref. number AP2009-3874) FPU, Ministerio de Educación, Cultura y Deporte, Spain. M. Aymerich acknowledges a Pre-Doctoral Fellowship from Xunta de Galicia (Spain) financed by the Secretaría Xeral de Universidades and Fondo Social Europeo. D. Nieto thanks to the Consellería de Cultura,Spain under the Galician Program for Research Innovation and Growth (2011–2015) (I2CPlan).

Author details

Ana Isabel Gómez Varela[1]*, María Aymerich[1], Daniel Nieto García[1], Yolanda Castro Martín[2], Pieter A.A. de Beule[3], Ezequiel Álvarez[4,5], Carmen Bao-Varela[1] and María Teresa Flores-Arias[1]

*Address all correspondence to: anaisabel.gomez@usc.es

1 Photonics4 Life Research Group, Department of Applied Physics, Faculty of Physics, University of Santiago de Compostela, Santiago de Compostela, Spain

2 Institute of Ceramics and Glass (CSIC), Kelsen 5, Campus de Cantoblanco, Madrid, Spain

3 Applied Nano-Optics Laboratory, International Iberian Nanotechnology Laboratory, Braga, Portugal

4 Health Research Institute of Santiago de Compostela (IDIS), University Hospital Complex of Santiago de Compostela (CHUS) SERGAS, Santiago de Compostela, Spain

5 CIBERCV, Madrid, Spain

References

[1] Klein LC. Sol-Gel Optics: Processing and Applications. Massachusetts: Springer Science & Business Media; 1994. DOI: 10.1007/978-1-4615-2750-3.

[2] Aegerter MA, Mennig M. Sol-Gel Technologies for Glass Producers and Users. New York: Springer Science & Business Media; 2004. DOI: 10.1007/978-0-387-88953-5.

[3] Reisfeld R. New materials for nonlinear optics. In: Jørgensen CK, Reisfeld R, editors. Optical and Electronic Phenomena in Sol-Gel Glasses and Modern Application. Structure and Bonding, **85**. Berlin: Springer; 1996. pp. 99–147. DOI:10.1007/BFb0111489.

[4] Rey-García F, Gómez-Reino C, Flores-Arias MT, Fuente GFDL, Durán A, Castro Y. Sol-gel coatings: an alternative route for producing planar optical waveguides. Thin Solid Films. 2011; **519**: 7982–7986. DOI: 10.1016/j.tsf.2011.05.054.

[5] Gómez-Reino C, Perez MV, Bao C. Gradient-Index Optics: Fundamentals and Applications. Berlin Heidelberg: Springer Verlag; 2002.

[6] Ohmi S, Sakai H, Asahara Y, Nakayama S, Yoneda Y, Izumitani T. Gradient-index rod lens made by a double ion-exchange process. Applied Optics. 1988; **27**: 496–499. DOI: 10.1364/AO.27.000496.

[7] Visconti AJ, Bentley JL. Fabrication of large-diameter radial gradient-index lenses by ion exchange of Na^+ for Li^+ in titania silicate glass. Optical Engineering. 2013; **52**: 112103–112103. DOI: 10.1117/1.OE.52.11.112103.

[8] Sinai P. Correction of optical aberrations by neutron irradiation. Applied Optics. 1971; **10**: 99–104. DOI: 10.1364/AO.10.000099.

[9] Pickering MA, Taylor RL, Moore DT. Gradient infrared optical material prepared by a chemical vapor deposition process. Applied Optics. 1986; **25**: 3364–3372. DOI: 10.1364/AO.25.003364.

[10] Yamane M, Yasumori A, Iwasaki M, Hayashi K. Graded index materials by the sol-gel process. In Proceedings of SPIE 1328, Sol-Gel Optics, 1 November 1990. pp. 133–144. DOI: 10.1117/12.22553.

[11] Laczka M, Wegrzynek JND, Wychowaniec M. GRIN glasses prepared by sol-gel method. In: Proceedings of SPIE 2943, Gradient-Index Optics in Science and Engineering, 22 October 1996. pp. 95–104. DOI: 10.1117/12.255522.

[12] Yeatman EM, Ahmad EM. Sol-gel fabrication of rare-earth doped photonic components. Journal of Sol-Gel Science and Technology. 2000; **11**: 231–236. DOI: 10.1023/A:1008792423076.

[13] Gonçalves RR, Messaddeq Y. Erbium-activated silica-zirconia planar waveguides prepared by sol-gel route. Thin Solid Films. 2008; **516**: 3094–3097. DOI: 10.1016/j.tsf.2007.07.183.

[14] Almeida RM, Marques AC. Rare earth-doped photonic crystals via sol-gel. Journal of Materials Science: Materials in Electronics. 2009; **20**: 307–311. DOI: 10.1007/s10854-008-9596-2.

[15] Gómez-Varela AI, Castro Y, Durán A, De Beule PAA, Flores-Arias MT, Bao-Varela C. Synthesis and characterization of erbium-doped SiO_2-TiO_2 thin films prepared by sol-gel and dip-coating techniques onto commercial glass substrates as a route for obtaining active gradient-index materials. Thin Solid Films. 2015; **583**: 115–121. DOI: 10.1016/j.tsf.2015.03.028.

[16] Gómez-Varela AI, Flores-Arias MT, Bao-Varela C, Gómez-Reino C. Focusing, collimation and beam shaping by active GRIN rod lenses: theory and simulation. Optics and Lasers in Engineering. 2012; **50**: 1706–1715. DOI: 10.1016/j.optlaseng.2012.07.011.

[17] Su L, Chen Y, Yi AY, Klocke F, Pongs G. Refractive index variation in compression molding of precision glass optical components. Applied Optics. 2008; **47**: 1662–1667. DOI: 10.1364/AO.47.001662.

[18] Kunnavakkam MV, Houlihan FM, Schlax M, Liddle JA, Kolodner P, Nalamasu O, Rogers JA. Low-cost, low-loss microlens arrays fabricated by soft-lithography replication process. Applied Physics Letters. 2003; **82**: 1152–1154. DOI: 10.1063/1.1555694.

[19] Fu YQ, Kok N, Bryan A. Microfabrication of microlens array by focused ion beam technology. Microelectronic Engineering 2000; **54**: 211–221. DOI: 10.1016/S0167-9317(00)00416-0.

[20] Pan CT, Wu TT, Chen MF, Chang YC, Lee CJ, Huang JC. Hot embossing of microlens array on bulk metallic glass. Sensors and Actuators A: Physical. 2008; **141**: 422–431. DOI: 10.1016/j.sna.2007.10.040.

[21] Wakaki M, Komachi Y, Kanai G. Microlenses and microlens arrays formed on a glass plate by use of a CO_2 laser. Applied Optics. 1998; **37**: 627–631. DOI: 10.1364/AO.37.000627.

[22] Delgado T, Nieto D, Flores-Arias MT. Soda-lime glass microlens arrays fabricated by laser: comparison between a nanosecond and a femtosecond IR pulsed laser. Optics and Lasers in Engineering. 2016; **86**: 29–37. DOI: 10.1016/j.optlaseng.2016.05.001.

[23] Nieto D, Arines J, Gomez-Reino C, O'Connor GM, Flores-Arias MT. Fabrication and characterization of microlens arrays on soda-lime glass using a combination of direct laser write and thermal reflow techniques. Journal of Applied Physics. 2011; **110**: 023108. DOI: 10.1063/1.3609085.

[24] Delgado T, Nieto D, Flores-Arias MT. Fabrication of microlens arrays on soda-lime glass using a laser direct-write technique and a thermal treatment assisted by a CO_2 laser. Optics and Lasers in Engineering. 2015; **76**: 1–6. DOI: 10.1364/AO.49.004979.

[25] McDonald JC, Whitesides GM. Poly (dimethylsiloxane) as a material for fabricating microfluidic devices. Accounts of Chemical Research. 2002; **35**: 491–499. DOI: 10.1021/ar010110q.

[26] Roman GT, Culbertson CT. Surface engineering of poly (dimethylsiloxane) microfluidic devices using transition metal sol-gel chemistry. Langmuir. 2006; **22**: 4445–4451. DOI: 10.1021/la053085w.

[27] Gomez-Sjoberg R, Leyrat AA, Houseman BT, Shokat K, Quake SR. Biocompatibility and reduced drug absorption of sol-gel-treated poly (dimethyl siloxane) for microfluidic cell culture applications. Analytical Chemistry. 2010; **82**: 8954–8960. DOI: 10.1021/ac101870s.

[28] Aymerich M, Gómez-Varela AI, Álvarez E, Flores-Arias MT. Study of different sol-gel coatings to enhance the lifetime of PDMS devices: evaluation of their biocompatibility. Materials. 2016; **9**: 728. DOI: 10.3390/ma9090728.

[29] Brinker CJ, Frye GC, Hurd AJ, Ashley CS. Fundamentals of sol-gel dip coating. Thin Solid Films. 1991; **201**: 97–108. DOI: 10.1016/0040-6090(91)90158-T.

[30] Bruynooghe S, Chabli A, Bertin F, Pierre F, Leflem G. Preparation and characterization of Nd^{3+} and Er^{3+}-doped silica sol-gel coatings by Rutherford backscattering spectroscopy and spectroscopic ellipsometry. Journal of Materials Research. 1997; 12: 2779–2783. DOI: 10.1557/JMR.1997.0370.

[31] Baklanov MR, Mogilnikov KP, Polovinkin VG, Dultsev FN. Determination of pore size distribution in thin films by ellipsometric porosimetry. Journal of Vacuum Science and Technology B. 2000; **18**: 1385–1391. DOI: 10.1116/1.591390.

[32] Skoczek E, Jaglarz J, Karasinsk P. Ellipsometric and spectrophotometric investigations of porous silica thin films produced by sol-gel method. Acta Physica Polonica A. 2011; **120**: 732–735. DOI: 10.12693/APhysPolA.120.732.

[33] Pilkington LAB. The float glass process. Proceeding of the Royal Society A. 1969; **314**: pp. 1–25. DOI: 10.1098/rspa.1969.0212.

[34] Nieto D, Arines J, Flores-Arias MT. Fluence ablation threshold dependence on tin impurities in commercial soda-lime glass. Applied Optics. 2014; **53**: 5416–5420. DOI: 10.1364/AO.53.005416.

[35] Nieto D, Flores-Arias MT, O'Connor GM, Gomez-Reino C. Laser direct-write technique for fabricating microlens arrays on soda-lime glass with a Nd:YVO_4 laser. Applied Optics. 2010; **49**: 4979–4983. DOI: 10.1364/AO.49.004979.

[36] Fiddes LK, Raz N, Srigunapalan S, Tumarkan E, Simmons CA, Wheeler AR, Kumacheva E. A circular cross-section PDMS microfluidics system for replication of cardiovascular flow conditions. Biomaterials. 2010; **31**: 3459–3464. DOI: 10.1016/j.biomaterials.2010.01.082.

[37] Ziober BL, Mauk MG, Falls EM, Chen Z, Ziober AF, Bau HH. Lab-on-a-chip for oral cancer screening and diagnosis. Head Neck. 2008; **30**: 111–121. DOI: 10.1002/hed.20680.

[38] Hongbin Y, Guangya Z, Siong CF, Shouhua W, Feiwen L. Novel polydimethylsiloxane (PDMS) based microchannel fabrication method for lab-on-a-chip application. Sensors and Actuators B: Chemical. 2009; **137**: 754–761. DOI: 10.1016/j.snb.2008.11.035.

[39] Xu BB, Zhang YL, Xia H, Dong WF, Ding H, Sun HB. Fabrication and multifunction integration of microfluidic chips by femtosecond laser direct writing. Lab on a Chip. 2013; **13**: 1677–1690. DOI: 10.1039/c3lc50160d.

[40] Stjernström M, Roeraade J. Method for fabrication of microfluidic systems in glass. Journal of Micromechanics and Microengineering. 1998; **8**: 33. DOI: 10.1088/0960-1317/8/1/006.

[41] Tsao CW, DeVoe DL. Bonding of thermoplastic polymer microfluidics. Microfluidics and Nanofluidics. 2009; **6**: 1–16. DOI: 10.1007/s10404-008-0361-x.

[42] Carlen ET, Bomer JG, van Nieuwkasteele JW, van den Berg A. Silicon and glass Micromachining. In: Herold KE, Rasooly A, editors. Lab-on-a-Chip Technology for Biomedical and Biological Applications. Volume 1: Fabrication and Microfluidics. Caister Academic Press, Norfolk, UK; 2009. pp. 83–114. ISBN: 978-1-904455-46-2.

[43] Li CW, Cheung CN, Yang J, Tzang CH, Yang M. PDMS-based microfluidic device with multi-height structures fabricated by single-step photolithography using printed circuit board as masters. Analyst. 2003; **128**: 1137–1142. DOI: 10.1039/B304354A.

[44] Bartholomeusz DA, Boutté RW, Andrade JD. Xurography: rapid prototyping of microstructures using a cutting plotter. Journal of Microelectromechanical Systems. 2005; **14**: 1364–1374. DOI: 10.1109/JMEMS.2005.859087.

[45] Etsion I. State of the art in laser surface texturing. Journal of Tribology. 2005; **127**: 248–253. DOI: 10.1115/1.1828070.

[46] Castelo A, Nieto D, Bao C, Flores-Arias MT, Pérez MV, Gómez-Reino C, López-Gascón C, De La Fuente GF. Laser backwriting process on glass via ablation of metal targets. Optics Communications. 2007; **273**: 193–199. DOI: 10.1016/j.optcom.2006.12.005.

[47] Estepa LC, De la Fuente GF. Continuous Furnace with Coupled Laser for the Surface Treatment of Materials. U.S. Patent 20090230105 A1, 7 March 2006.

[48] Rodiño-Janeiro BK, González-Peteiro M, Ucieda-Somoza R, González-Juanatey JR, Álvarez E. Glycated albumin, a precursor of advanced glycation end-products, up-regulates NADPH oxidase and enhances oxidative stress in human endothelial cells: Molecular correlate of diabetic vasculopathy. Diabetes-Metabolism Research and Reviews. 2010; **26**: 550–558. DOI: 10.1002/dmrr.1117.